Journal of Engineering Science and Technology
Vol. 15, No. 4 (2020) 2472 - 2491

A NUMERICAL STUDY OF NATURAL CONVECTION IN SQUARE CAVITY WITH HEATED CYLINDER OF DIFFERENT DIAMETER AND LOCATION THROUGH COMPUTATIONAL ANALYSIS

AMEER ABED JADDOA [1,*], ALI L. EKAID[2], LAITH AL-SADAWI[3]

[1] Department of Electromechanical Engineering, University of Technology, Baghdad, Iraq
[2, 3] Department of Mechanical Engineering, University of Technology, Baghdad, Iraq
*Corresponding Author: 50087@uotechnology.edu.iq

Abstract

In the current study, the effect of an inner heated circular cylinder placed inside a cooled square enclosure on the heat transfer and fluid flow is numerically studied. The main parameters that were investigated are the position of the inner cylinder which was varied both in the vertical and diagonal directions from -0.2 to +0.2 and the aspect ratio which was from 0.05 to 0.25. The Rayleigh number and the Prandtl number were kept constant at 10^6 and 0.7, respectively. However, for the comparison study, three Prandtl numbers were examined 10^4, 10^5, and 10^6. The numerical study is conducted using (FORTRAN 90) code which is built to perform the calculations for the Navier-Stokes equation of the stream-vorticity expression using finite-difference approach that relates with the non-orthogonal body-fitted coordinate system. The results revealed that the highest local Nu number was achieved at the top surface of the cylinder when the cylinder is moved both in the vertical and diagonal direction. In addition, when the aspect ratio increases the average Nusselt Number increases.

Keywords: Diagonal and vertical location, Different diameters, Heated cylinder, Natural convection.

1. Introduction

Natural convection heat transfer in an enclosure is of immense importance for many engineering applications such as heat exchangers, reactors, cooling of electronic components, and underground transmission lines. Until recently, numerous researchers have investigated the four-sided enclosure with embedded objects inside the enclosure. The current study focuses on the effect of both the inner cylinder's diameter and location on the natural convection heat transfer generated from an inner circle-shaped cylinder within a four-sided cold enclosure. Several studies have examined the effect of various inner body shapes under different thermal conditions within a square enclosure. For instance, many studies focused on the effect of both vertically [1-5]. Another researcher has focused on horizontally imposed temperature [6-10]. In addition, a lot of investigations have been focused on effect of the position of the inner body that is either concentric or eccentric within an enclosure on the natural convection heat transfer.

Cho et al. [11] numerically studied natural convection heat transfer inside concentric and eccentric annuli. They found that for a Rayleigh numbers less than 5×10^4, the thermal behaviour for the annuli with very small eccentricity was similar to that of the concentric one. Moreover, a maximum deviation of 5 percent was shown in the local heat transfer of the cylinder wall. For Rayleigh numbers up to 10^6, Asan [12] investigated the natural convection heat transfer in a square annulus between two concentric horizontal square cylinders. The results proved the effect of the aspect ratio and the Rayleigh number on the flow field and temperature within the annuli. Arnab and Amaresh [13] studied the effect of tilted, heated, square cylinder inside a square enclosure for Rayleigh numbers between 10^3 and 10^6. They reported that for different aspect ratios, both flow field and the thermal characteristics were significantly modified. In addition, the overall heat transfer coefficient is related to the change in the aspect ratio.

Moreover, many researchers have investigated the thermal influence of the natural convection heat transfer characteristics that occur due to the presence of heated inner body within cooled enclosure. Nasrine and Ghaddar [14] conducted a numerical study of natural convection heat transfer generated by heated circular cylinder placed inside a large rectangular enclosure. The reported results showed that the applied heat flux on the inner cylinder affects the thermal behaviour. In addition, they found that both Nu and Ra are correlated according to a general form $Nu_a = C1\ (Ra_a)^{c2}$.

Moukalled and Acharya [15] investigated the effect of different aspect ratios of cylinder radius to the enclosure height for a Rayleigh numbers that range from 10^4 to 10^7. They reported that the total heat transfer increased as the Rayleigh number increased for a constant aspect ratio. Ding et al. [16] conducted a numerical investigation on the effect of eccentricity on the natural convection heat transfer between heated circular within a square enclosure at Rayleigh number 3×10^5. They reported that separation, circulation pockets and aspect ratio had a profound effect on the thermal behaviour inside the annulus between the inner cylinder and the outer enclosure.

For different Rayleigh numbers, the effect of temperature difference between a cold outer square enclosure and heated circular cylinder that is placed at different vertical positions on the natural convection heat transfer was reported by Kim et al. [17]. The internal cylinder location and Rayleigh number were found to have a profound effect on both the size and number of the convection cells. Lee et al. [18],

study the natural convection heat transfer induced by a hot inner cylinder and cold outer enclosure. The cylinder has a fixed aspect ratio and placed at different diagonal and horizontal locations. They reported that local peaks of Nusselt number exist along the surface of the inner cylinder and outer enclosure.

Recently researchers have investigated the effect of natural convection with porous and nano-fluid are presented in the annulus region between an enclosure and a circular cylinder. For example, Abdulkadhim et al. [19] studied the effect of an adiabatic Circular cylinder on the natural convection heat transfer in an enclosure with a porous media inside. They found that as the Rayleigh number increases the rate of heat transfer increases. Ali et al. [20] investigated the effect nano-fluid layers between a rotated outer circular cylinder and a corrugated inner cylinder. They found that the average and decreases with the higher the Reynolds number the lower the average Nusselt number. The opposite is true for the Rayleigh number.

More recent, Abdulkadhim et al. [21] examined the effect of both porous-nano fluids on the heat transfer between a corrugated inner cylinder and a wavy enclosure. They reported that increasing the layers of the porous media results in a reduction in the heat transfer.

There has been little attention on the effect of the eccentricity in the diagonal and vertical directions with different aspect ratios on the natural convection heat transfer in an annulus between circular, heated inner cylinder within outer cold enclosure. The current work will focus on the effect of various aspect ratios along with position of the inner body in the vertical and diagonal direction on both thermal behaviour and the fluid flow field.

2. Physical Specifications

Figure 1 shows the problem that this work considers. A Newtonian viscous fluid that is incompressible is considered between a two-dimensional four-sided enclosure and a circular cylinder. The enclosure's width and height is *(L).* The cylinder radius is *(R).* The square enclosure is filled with air as a working fluid with Prandtl number of *(Pr =0.7).* The walls temperatures of the square enclosure are kept cooled at (T_c), while surface of the cylinder is uniformly heated at (T_h). The radius *(R)* of circular cylinder is located and moves along the vertical centreline and diagonal of enclosure in the range from (-0.2 to +0.2).

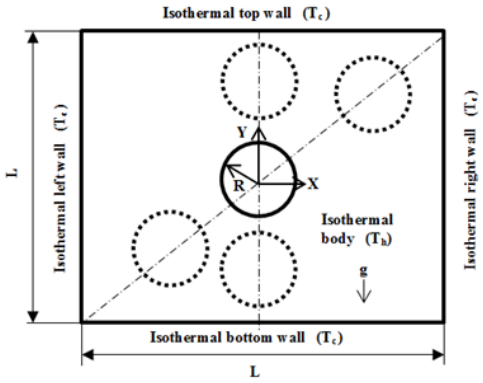

Fig. 1. Computational zone and coordinate system with boundary conditions used.

2.1. Mathematical formulation of governing equation

Streamfunction-vorticity formulation is used to write the fluid flow governing equations, and heat transfer in two dimensions covering questions as shown below. To obtain these questions, Boussinesq approximation was invoked.

$$\omega_t + (u\omega)_x + (v\omega)_y = \nu\left(\omega_{xx} + \omega_{yy}\right) + \beta g T_x \tag{1}$$

$$T_t + (uT)_x + (vT)_y = \alpha\left(T_{xx} + T_{yy}\right) \tag{2}$$

$$\psi_{xx} + \psi_{yy} = -\omega \tag{3}$$

$$u = \psi_y, v = -\psi y \tag{4}$$

Figure 1 describes the physical problem shows boundary conditions relevant to the study in hand. To convert the above equations to dimensionless, the following scales are taken:

$$\begin{aligned} &x^* = \frac{x}{L},\ y^* = \frac{y}{L},\ u^* = \frac{uL}{\alpha},\quad v^* = \frac{vL}{\alpha},\quad t^* = \frac{\alpha t}{L^2} \\ &\omega^* = \frac{\omega L^2}{\alpha},\ \psi^* = \frac{\psi}{\alpha},\ \theta = \frac{T - T_c}{T_h - T_c} \end{aligned} \tag{5}$$

For Case 1 and $\theta = \frac{T-T_c}{q_o L}$ for Case 2 depends on the coordinates of curvilinear $x = x(\xi,\eta), y = y(\xi,\eta),$

The transformed equations of non-dimensional are Arnab and Amaresh [13]:

$$\omega t + \frac{1}{J}\left((U\omega)_\xi + (V\omega)_\eta\right) = Pr\nabla^2\omega + \frac{1}{J} Ra\, Pr\, (y_\eta\theta_\xi - y_\xi\theta_\eta) \tag{6}$$

$$\theta_t + \frac{1}{J}\left((U\theta)_\xi + (V\theta)\eta\right) = \nabla^2\theta \tag{7}$$

$$\nabla^2\psi = -\omega \tag{8}$$

$$u = \frac{1}{J}\left(-x_\eta\psi_\xi + x_\xi\psi_\eta\right), v = \frac{1}{J}\left(-y_\eta\psi_\xi + y_\xi\psi_\eta\right) \tag{9}$$

where $U = y_\eta u - x_\eta v$ and $V = -y_\xi u + x_\xi v$ are the contra variant velocity components in directions, respectively. J is the transformation of the Jacobian defined as $J = x_\xi y_\eta - y_\xi x_\eta$ which is the Laplacian of a generic scalar in the transformed plane is presented as

$$\nabla^2\phi = \frac{1}{J^2}(\alpha\phi_{\xi\xi} + \beta\phi_{\xi\eta} + \gamma\phi_{\xi\xi}) + \frac{1}{J^3}/\left[\left(-y_\eta A + x_\eta B\right)\phi_\xi + \left(y_\xi A - x_\xi B\right)\phi_\eta\right] \tag{10}$$

where:

$$\alpha = x_\eta^2 + y_\eta^2, \gamma = x_\xi^2 + y_\xi^2, \beta = -2\left(x_\xi x_\eta + y_\xi y_\eta\right),$$

$$A = \alpha x_{\xi\xi} + \beta x_{\xi\eta} + \gamma x_{\eta\eta} and$$
$$B = \alpha y_{\xi\xi} + \beta y_{\xi\eta} + \gamma y_{\eta\eta}.$$

The coefficient of the heat transfer is articulated as

$$h = \frac{q}{T_H - T_C} \tag{11}$$

A nondimensional heat transfer coefficient known as Nusselt number Nu is calculated as shown in Eq. (12).

$$Nu = \frac{hD}{K} \tag{12}$$

The thermal conductivity is articulated as

$$k = \frac{-q}{\partial T/\partial n} \tag{13}$$

The stream function (ψ) and vorticity (ω) in the governing equations are defined as follows:

$$u = \frac{\partial \psi}{\partial y},\ v = -\frac{\partial \psi}{\partial x},\ \omega = \frac{\partial v}{\partial x} - \frac{\partial u}{\partial y} \tag{14}$$

The flow initial conditions between vented enclosure and heated cylinder are:

$$\psi = 0\ , \theta = 0, \omega = 0\ for\ t = 0 \tag{15}$$

Temperature boundary conditions are:

$$\theta = 1 \qquad \text{Inner cylinder wall} \tag{16a}$$

$$\theta = 0 \qquad \text{Outer cylinder wall} \tag{16b}$$

Vorticity boundary conditions are:

$$\omega = \frac{2\gamma}{J^2(\psi_{i,1} - \psi_{i,2})} \tag{17a}$$

$$\omega = \frac{2\gamma}{J^2(\psi_{i,m} - \psi_{i,m-1})} \tag{17b}$$

Local Nusselt number at the inner and outer cylinder has been calculated be the following expression:

$$Nu_h = \frac{1}{J\sqrt{\alpha}}(\alpha T_\xi + \gamma T_\eta) \tag{18a}$$

$$Nu_c = \frac{1}{J\sqrt{\alpha}}(\alpha T_\xi - \gamma T_\eta) \tag{18b}$$

The Average Nusselt number on the inner and outer cylinder wall is evaluated as:

$$\overline{Nu}_h = \int_0^{2\pi} \frac{\partial \theta}{\partial n} \partial \xi \tag{19a}$$

$$\overline{Nu}_c = \int_0^{4L} \frac{\partial \theta}{\partial n} \partial \xi \tag{19b}$$

where $\partial \xi$ At surface of the cylinder.

The mentioned above numerical algorithm was executed via building computer program in (Fortran 90) which is suitable to express a natural convection from a cylinder that is heated and placed inside an enclosure.

2.2. Numerical technique

The false transient alternating direction implicit (ADI) method was used to solve the vorticity transport equation and the energy equation, and the successive over relaxation (SOR) method was utilized to solve the stream function equation.

2.3. Grid generation

One of the assumptions in this study is the grids generation of the curvilinear body-fitted at coordinates by:

$$\nabla^2\xi = p(,\eta) \tag{20}$$

$$\nabla^2\eta = Q(\xi,\eta) \tag{21}$$

where P & Q refer to the control functions that required to retain the wanted in domain grid density. By using physical coordinates as the dependent variables, Eqs. (20) and (21) can be formed as follow:

$$\alpha x\xi\xi + \beta x\xi\eta + \gamma x\eta\eta + J^2(px\xi + Qx\eta) = 0 \tag{22}$$

$$\alpha y\xi\xi + \beta y\xi\eta + \gamma y\eta\eta + J^2(py\xi + Qy\eta) = 0 \tag{23}$$

In the current work, elliptic grid technique is implemented as the control function in order to maintain the desired grid density and to avoid poor grid quality especially near the cylinder wall [22]. SOR method was used to solve both Eqs. (22) and (23). By using second order central difference scheme, all the derivatives are discretized, and the non-linearity is dealt with by iterations. Examples on the resulted grids for the inner cylinder at different locations are demonstrated in Fig. 2.

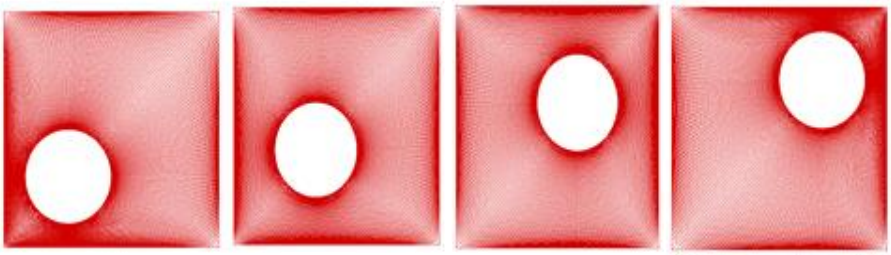

Fig. 2. A typical numerical grid (200 ×100).

2.4. Solution procedure

Since the boundaries of the domain do not lie along natural coordinates, a boundary-fitted non-orthogonal coordinate system is used. The solution procedure involves grid generation, discretization of the governing equations, and an algorithm for solving the equations.

2.5. Discretization of conservation equations

The finite difference technique in the transformed plane is adapted to solve the governing equations (9) and (6). The standard central scheme is utilized in the convective terms in the two transport equations, while the second order central difference scheme is used for performing the spatial discretization. In the current work, a semi-implicit time integration scheme is implemented for both vorticity and temperature values. The no-linear convective terms in vorticity and energy equations are linearized in Eqs. (24) and (25):

$$J\frac{\theta_{i,j}^{n+1}}{\Delta t} + (U^n\theta^{n+1})_{i,j} + (V^n\theta^{n+1})_{i,j} = J(\nabla\theta^{n+1})_{i,j} \tag{24}$$

$$J\frac{\omega_{i,j}^{n+1}+\omega_{i,j}^{n}}{\Delta t}+(U\omega_{n+1})_{i,j}+(V^{n}\omega^{n+1})_{i,j}=J\,Pr(\nabla^{2}\omega^{n+1})_{i,j}+JRa\,Pr(y_{\eta}\theta_{\xi}-y_{\xi}\theta_{\eta})_{i,j}^{n+1} \quad (25)$$

In the above equations, the definition of the Laplacian term is given in Equation (10). Equations (24) and (25) are solved using SOR method in order to get the discretized form of the equations. This technique is chosen because it converges fast with only a few iterations especially for cylinder at diagonal locations. The resulted linearized equations from the discretized Poisson equation for the stream function are dealt with using the Bi-Conjugate Gradient technique [24].

2.6. Study of grid independency and stability

In the present study, the stability of the numerical prediction and the grid independency are examined for the case Ra=10^6 and Pr = 0.7 for all aspect ratios R/L considered in this work. The time steps are chosen with values 0.01.The grid-independence of numerical results is studied for the all cases. Three mesh sizes of 150×75, 175×75 and 200×100 are generated to check the grid-independency. For all the examined meshes the total numbers of the grid nodes are 11250, 13125, and 20000, which correspond to the 150×75, 175×75 and 200×100 mesh size, respectively as shown in Fig. 3. The 200×100 mesh size is chosen for all the tested cases as a stabilized Nusselt number is obtained.

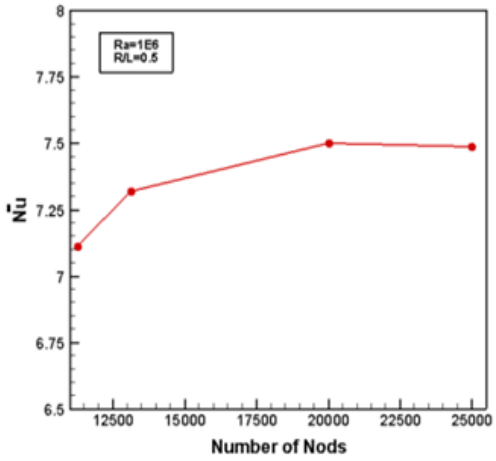

Fig. 3. Mesh independency test.

3. Model Validation

Comparison of the average Nusselt number that is calculated in the current study with the numerical results reported by Moukalled et al. [15] and Ding et al. [16] was performed as well at three different Ra numbers (10^4, 10^5, and 10^6). They conducted a *2D* numerical analysis on natural convection heat transfer between heated eccentric inner cylinder and cooled enclosure. The average Nusselt Number from both studies compared to the current study is presented in Fig. 4. It can be seen that the agreement between the results in the current study and the numerical prediction reported in [15, 16] as well. Figure 5 shows a comparison between the

isotherm and stream lines in the current study with the reported results in Moukalled et al. [15].

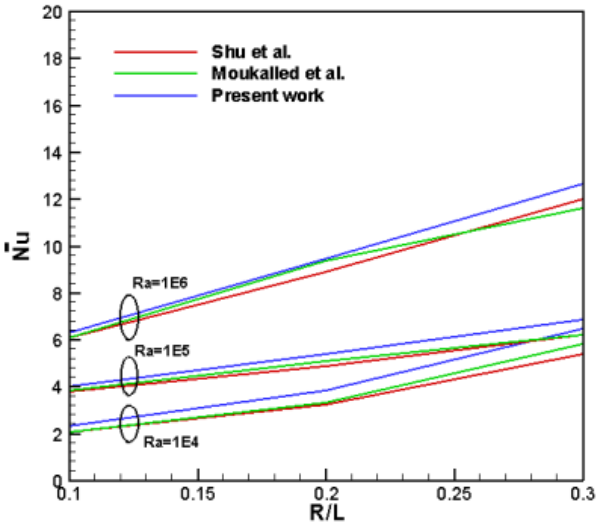

Fig. 4. Comparison of current average Nusselt Number with reported results in [15, 16].

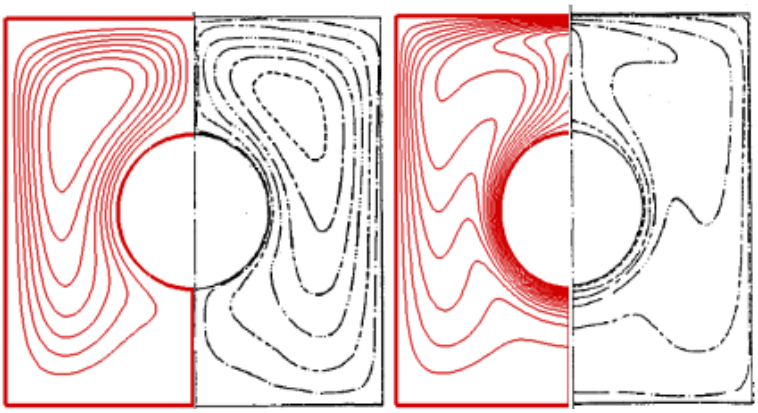

Fig. 5. Comparison of stream and temperature contour for Ra=1E6 and R/L=1 with [15].

4. Results and Discussion

In the next sections, the results for different geometrical cases that are considered in the current investigation are demonstrated. Two geometrical parameters are considered these are the aspect ratio ($0.05 \leq R/L \leq 0.25$) and inner heated body position which changes in both vertical and diagonal directions. The thermal boundary conditions in the current study are kept fixed, where the inner body is heated while the outer enclosure is cooled. In the current numerical study, the working fluid in the annuli region is air with a Prandtl number and Rayleigh number of 0.7 and 10^6, respectively. Both fluid flow and heat transfer characteristics are

explained with the help of streamlines and temperature contours, respectively. Finally, in order to evaluate the overall heat transfer performance, both local and averaged Nusselt numbers on hot and cold surfaces are plotted.

4.1. Fluid flow and heat transfer characteristics

In this section both fluid and heat transfer properties represented by the streamlines and isotherms are presented. The streamlines and temperature contours for different aspect ratios when the position of the inner cylinder was changed in the vertical direction are depicted in Figs. 6-10.

From Fig. 6, when the cylinder is in the middle of the outer enclosure (Y/L = 0), the streamlines and the isotherms show that the hot flow tends to move upward due to thermal expansion along the vertical symmetry line. As the air impinges on the upper wall it becomes colder and denser thus it moves radially away from the top wall and downward again. Thus, two recirculation air pockets are formed on the sides of the vertical symmetry line with center of the recirculation close to the upper part of the enclosure. As the aspect ratio increases and for the highest aspect ratio examined (R/L= 0.25), a distortion in the isotherm patterns can be seen. Flow separation in the upper annuli occurs and two thermal plums are formed. In addition, the recirculation has two eddies, a big one rotates anticlockwise and small one rotates in the clockwise direction, which agrees with the reported observation in Moukhalled et al. [15].

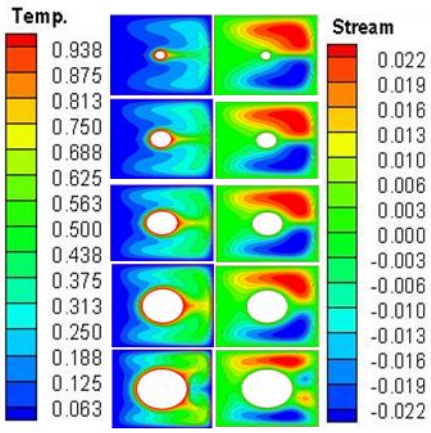

Fig. 6. Fluid flow and isotherms contours for Y/L =0 and 0.05 ≤ R/L≤ 0.25.

The effect of moving the center of the cylinder vertically is shown in Figs. 6-10. When the center of the inner cylinder is vertically moved above the center of the enclosure Figs. 7 and 8, one can see that the flow and isotherms contours behave similarly to the previous case when the cylinder is positioned at (Y/L = 0) especially at low aspect ratios ($R/L \leq 0.15$). At (Y/L = 0.1) and higher aspect ratios (R/L = 0.2 and 0.25), the flow separates earlier compared with the previous case when the cylinder is placed in the middle as shown in Fig. 6. In addition, the stream lines show the occurrence of pair of secondary vortices close to the upper wall of the enclosure. This observation agrees well with the reported results in Kim et al. [17] for Ra = 106 and for 0.2 aspect ratio where they found that secondary vortices are

formed near the upper wall. However, when the cylinder is placed (Y/L = 0.2) (the closest position to the upper wall), the flow tends to separates at aspect ratios ($R/L \geq 0.15$). One can also notice that the small eddies near the top wall disappear when the cylinder at the closest position to the upper wall as can be seen in Fig. 8.

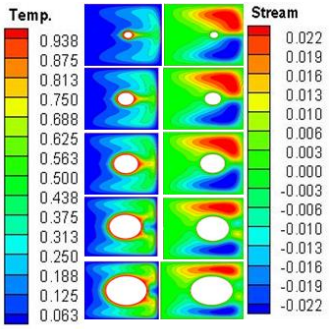

Fig. 7. Fluid flow and isotherms contours for Y/L =0.1 and 0.05 ≤ R/L≤ 0.25.

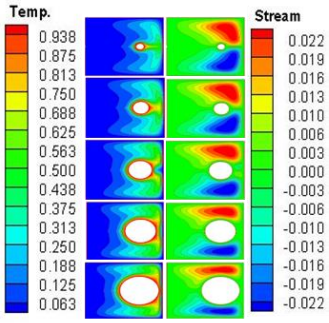

Fig. 8. Fluid flow and isotherms contours for Y/L =0.2 and 0.05 ≤ R/L≤ 0.25.

As the cylinder is moved downward where the center of the inner cylinder is below the center of the outer enclosure (Y/L = -0.1and -0.2), the flow dose not separate and central and large plumes occur which pump the hot air toward the upper wall along the vertical symmetry line for all the examined aspect ratios as shown in Figs. 9 and 10. This observation also agrees with the reported results by Kim et al. [17] where they reported that the secondary vortices close to the upper wall disappear as the distance between the inner cylinder and the upper wall increases.

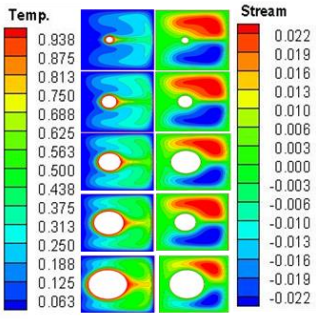

Fig. 9. Fluid flow and isotherms contours for Y/L = -0.1 and 0.05 ≤ R/L≤ 0.25.

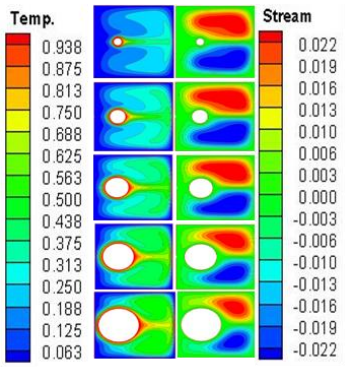

Fig. 10. Fluid flow and isotherms contours for Y/L = -0.2 and $0.05 \leq R/L \leq 0.25$.

In addition to the effect of changing the position of the inner cylinder vertically, the effect of changing the aspect ratio and cylinder's position diagonally was also examined Figs. 11-14.

From Fig. 11, one can notice that the strength of the thermal plume increases as the aspect ratio increases because the space between the cylinder and the enclosure's top and right walls becomes smaller for ($R/L \leq 0.1$). As the aspect ratio increases more ($R/L \geq 0.15$), the distance between the cylinder and the enclosure walls becomes smaller. Thus, the two thermal plumes occurs for (R/L = 0.15) then disappear for (R/L = 0.25). One can also notice from the streamlines contours, that as the aspect ratio increases, a secondary eddy occurs within the primary one at the right side of cylinder for ($R/L \geq 0.15$). When the cylinder is moved slightly above the centre of the enclosure along the diagonal line at (X/L = 0.1, Y/L = 0.1), the thermal plume becomes stronger than what is seen in the previous location as the distance between the cylinder and the enclosure upper and right walls becomes larger. The thermal plume separation occurs at ($R/L \geq 0.2$) compared to ($R/L \geq 0.15$) for the previous location. As the inner cylinder moves further from the right-upper corner to the left-lower corner of the enclosure, the space between the cylinder and the right quarter of the enclosure increases. Thus, the convection due to buoyancy effect is enhanced.

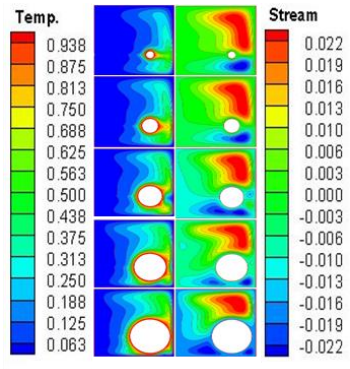

Fig. 11. Fluid flow and isotherms contours for Y/L = 0.2 and $0.05 \leq R/L \leq 0$.

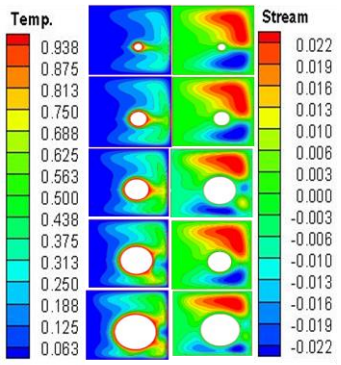

Fig. 12. Fluid flow and isotherms contours for $Y/L = 0.1$ and $0.05 \leq R/L \leq 0.25$.

As a result, large upward plume occurs at the top of the inner cylinder especially when the cylinder is placed below the centres of the enclosure as can be seen in Figs. 13 and 14. From the streamlines contours, one can also notice that for ($R/L \geq 0.15$), a secondary eddy occurs with the primary one on the left side of the inner cylinder as the distance between the cylinder and the left side of the enclosure becomes smaller as can be seen in Fig. 14. In Fig. 14, it can be seen that for ($R/L \leq 0.15$), the secondary eddy occurs within the primary one on the left side of the enclosure. Then, this secondary eddy merges into one primary eddy for ($R/L \geq 0.2$)

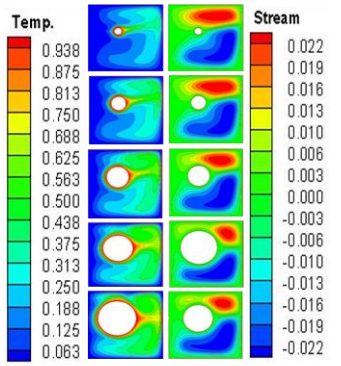

Fig. 13. Fluid flow and isotherms contours for $Y/L = -0.1$ and $0.05 \leq R/L \leq 0.25$.

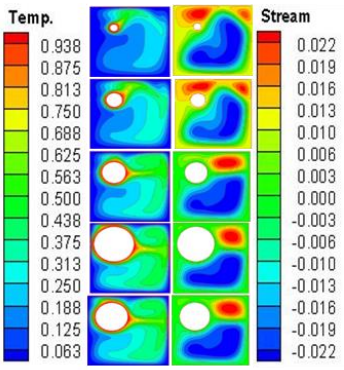

Fig. 14. Fluid flow and isotherms contours for $Y/L = -0.2$ and $0.05 \leq R/L \leq 0$.

4.2. Local and average Nusselt numbers

In addition to the fluid flow and isotherms, the local and average Nusselt numbers $Nu_{c,h}$ and , respectively were also calculated for both cooled and heated surfaces. The distribution of the local Nu for the heated cylinder and cooled enclosure is depicted in Fig. 15 for different vertical locations. When the inner cylinder is at the centres of the square enclosure and the aspect ratios ($R/L \leq 0.2$), the minimum Nu_h is seen at the top of the cylinder surface where the plum occurs, and the isotherm contours are coarsest as shown in Fig. 6. The largest Nu_h is shown to be at ($\theta = 0^o$ and 360^o), where the temperature contours are densest due to the movement of the upward directed cold fluid. As the aspect ratio increases above ($R/L = 0.25$), the location of the minimum Nu_h is shown at location $\theta = 144^o$ and 210^o where the two plums occur as shown in Fig. 6. However, the maximum Nu_h is seen for the aspect ratio ($R/L = 0.25$) at the region between the two plums where the temperature gradient is the highest. As the inner cylinder moves vertically above and below the centres of the enclosure, the maximum Nu_h is seen when the cylinder is placed close to the top wall ($Y/L > 0$) of the enclosure ($\theta = 180^o$). However, for ($Y/L < 0$), the maximum Nu_h is found to be at ($\theta = 0^o$ and 360^o) as shown in Fig. 15. For the cooled enclosure, when the cylinder is at the centres of the enclosure, the lowest Nu_c is found at the corners of the enclosure for all of the tested aspect ratios except for ($R/L = 0.25$) where in addition to the corners a low Nu_c can also be seen at the centres of the top wall. The maximum Nu_c is found to be at the centres of the upper wall and slightly below the top corners for ($R/L \leq 0.2$). As the cylinder centres is moved below the centres of the enclosure ($Y/L < 0$), the maximum Nu_c is found to be not only at the centres of the upper wall and slightly below the upper corners but also at centres of the bottom wall when the cylinder at the closest position to bottom of the enclosure. For ($Y/L > 0$), the lowest Nu_c is shown to be at the corners of the enclosure and the centres of the upper wall for ($R/L \geq 0.2$) and ($1.5 \leq R/L \leq 0.2$) at ($Y/L = 0.1$) and ($Y/L = 0.2$), respectively, as shown in Fig. 15 (right column). Figure (left column) shows the distribution of the Nu_h on the surface of the heated cylinder when its position is changed in the diagonal direction. From Fig. 14 one can notice that the maximum Nu_h is found to be at the right and left sides of the cylinder ($360^o \leq \theta < 180^o$) for ($Y/L < 0$), while for ($Y/L > 0$), the highest Nu_h is seen close to the left side of the cylinder due to the distortion in the isotherm contours as shown in Figs. 11-14. One can also notice that the highest peaks of the Nu_h are seen between the two plums where the flow separates.

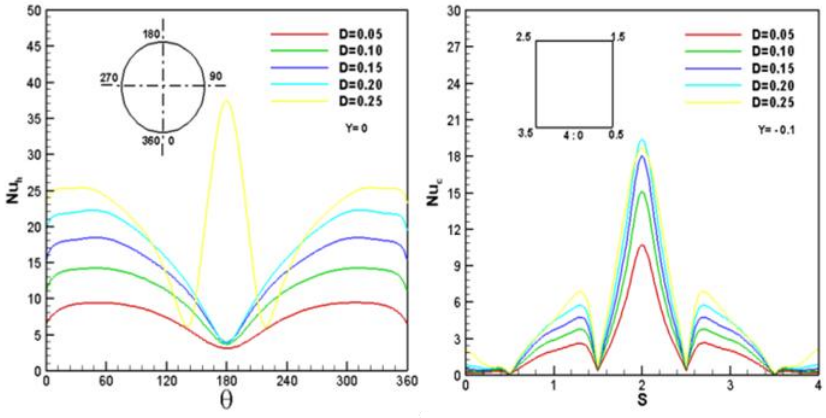

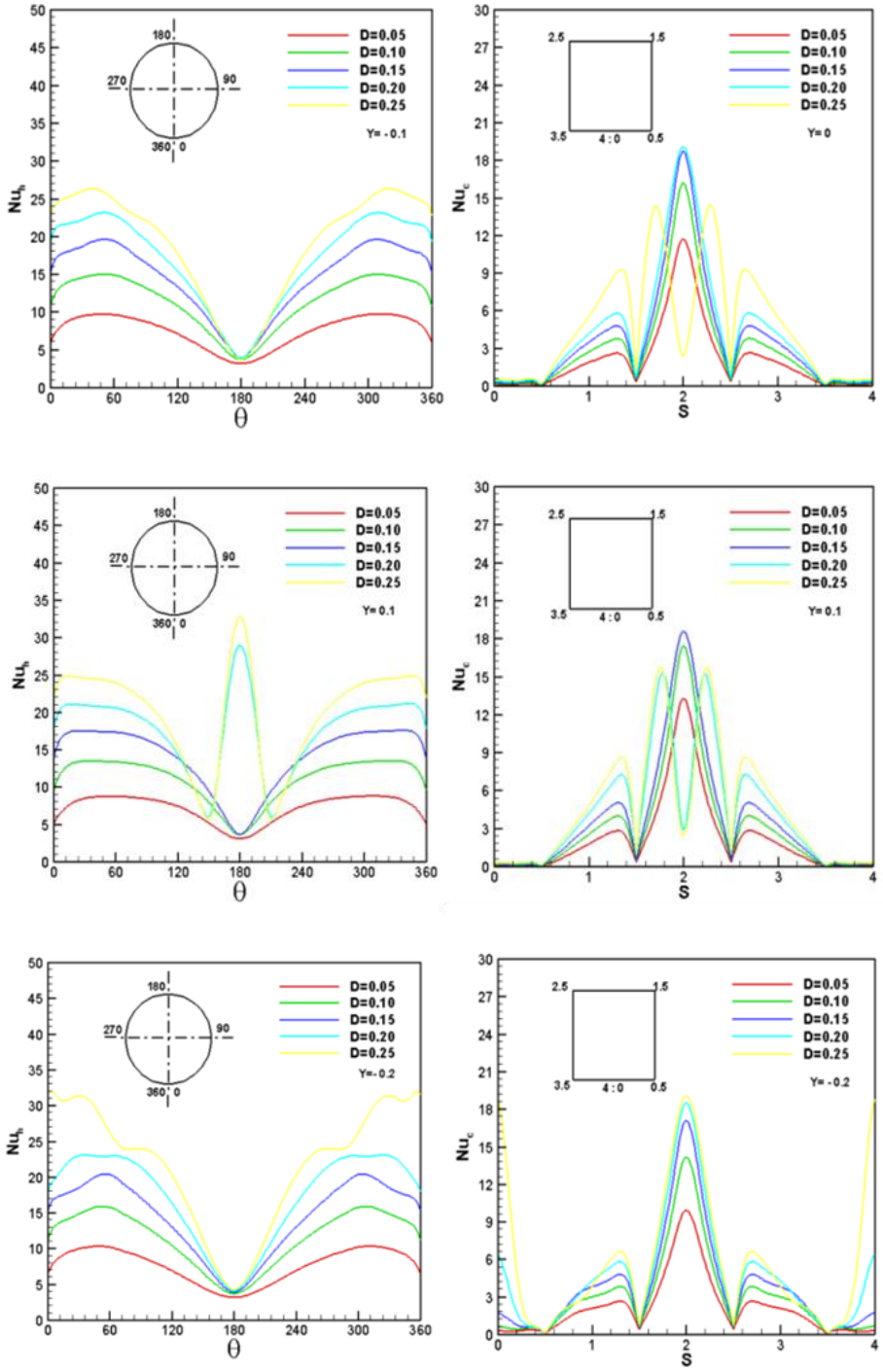
D=0.05
D=0.10
D=0.15
D=0.20
D=0.25
Y= - 0.1
Y= 0
Y= 0.1
Y=- 0.2
Nu_h
Nu_c
θ
S
180
270
90
360 0
2.5
1.5
3.5
0.5
4 : 0

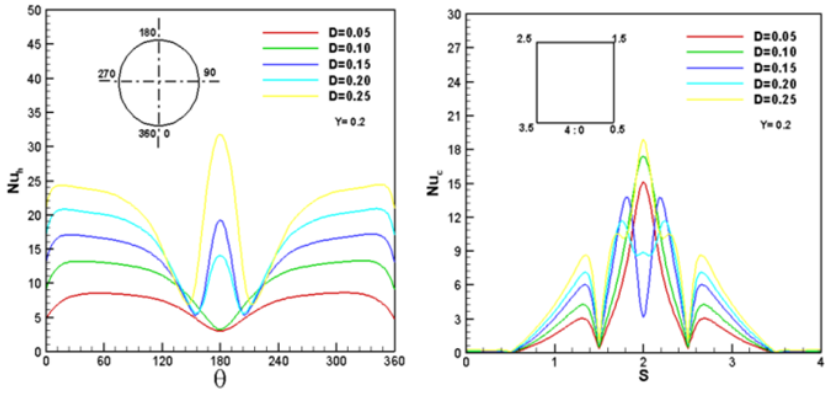

Fig. 15. Local Nusselt Number for hot and cold surfaces vertical location.

The variation of the Nu_h along the walls of the cooled enclosure is shown in Fig. 16 (right column). When the inner cylinder is located close to the right and left walls of the enclosure, the highest Nu_c is achieved due to the dominance of conduction at these locations. For the ($Y/L > 0$ and $Y/L < 0$), the minimum Nu_c is found to be near the corners of the enclosure.

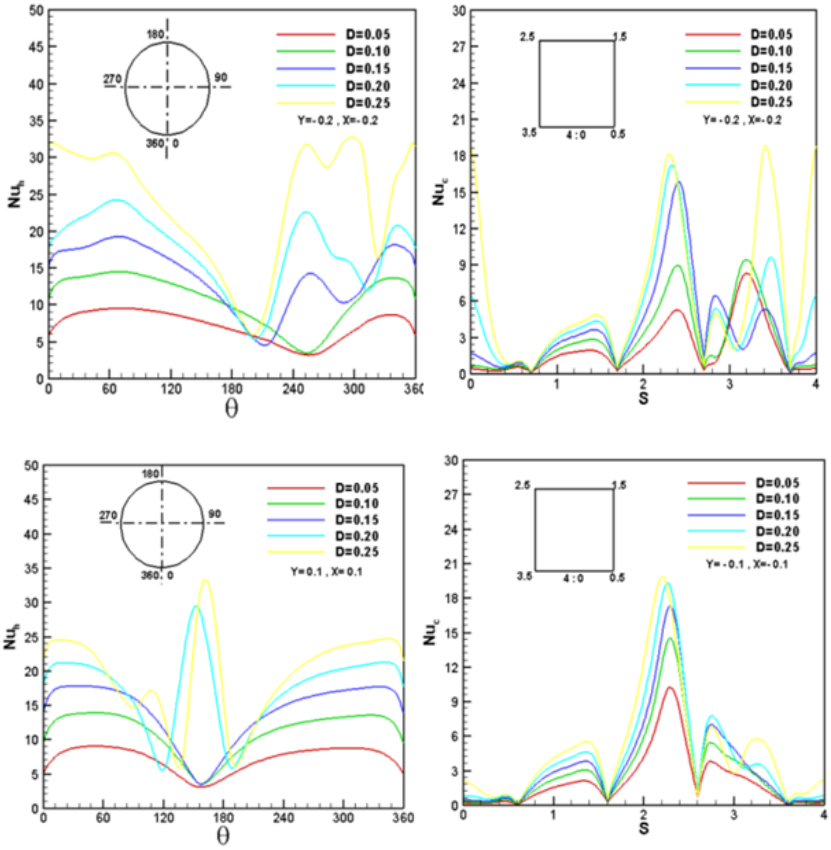

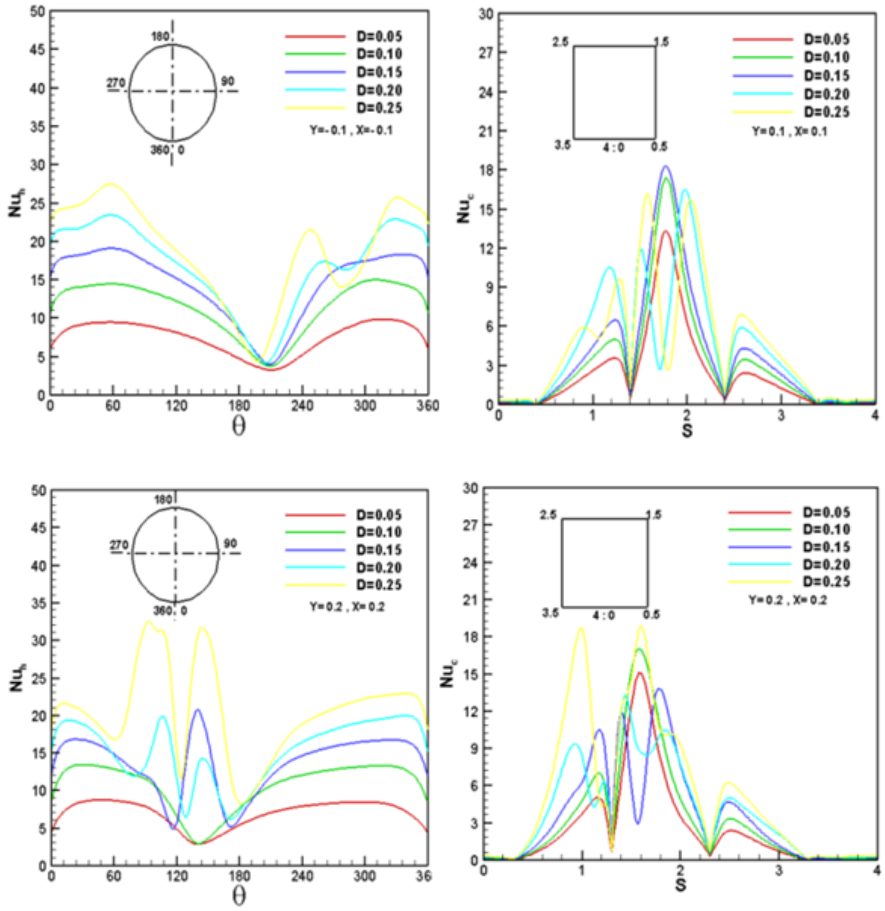

Fig. 16. local Nusselt number for hot and cold surfaces diagonal location.

In addition to the local Nusselt Number $Nu_{h,c}$, the average surface Nusselt number $\overline{Nu}$ is also used to characterize the effect of the aspect ratio on the natural convection heat transfer that is induced by the temperature difference. Figure 17 (A & B) presents the distribution of $\overline{Nu}$ along the surface of the heated inner cylinder and the cooled outer enclosure for different aspect ratios in the vertical and diagonal directions.

The results reveal that as the aspect ratios *(R/L)* increase the $\overline{Nu}$ values for the both hot and cold surfaces increase. This observation agrees with the results presented in Moukalled et al. [15] who reported that for a constant Rayleigh number, the average $\overline{Nu}$ increases as the aspect ratio increases. One can also notice that changing the place of inner cylinder has a slight effect on the overall heat transfer for both hot and the cold surfaces

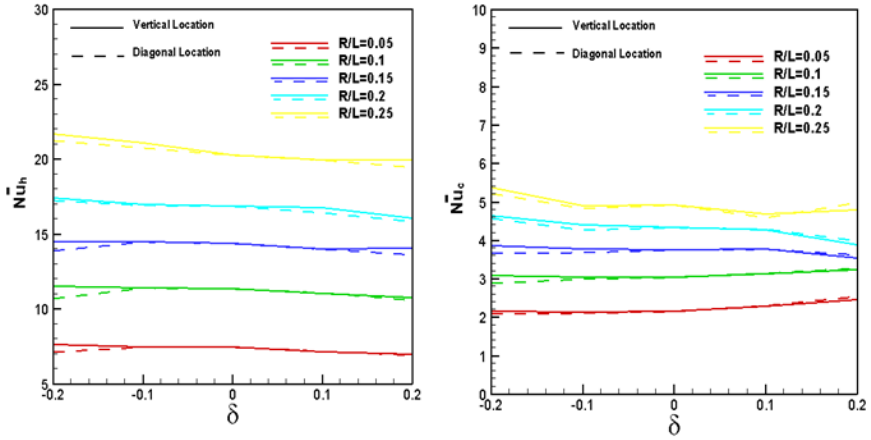

Fig. 17. A & B average Nusselt Number for hot and cold surfaces.

5. Conclusion

The effect of a heated inner circular cylinder that is located at various positions along the vertical and diagonal line of cooled square outer enclosure on the heat transfer convection is investigated.

The Rayleigh and Prandtl numbers were fixed at 10^6 and 0.7, respectively. For mesh independency test, Rayleigh number of 10^6 was chosen. In order to compare with previous studies, a Rayleigh number of 10^6 were used. Fluid flow and heat transfer simulation is achieved using stream- vorticity method in the curvilinear coordinates.

The results showed that when the cylinder center is changed along the vertical line of the enclosure, two large symmetrical eddies occur on both sides of the inner heated cylinder especially when the cylinder at the Centre. However, the eddies become smaller and closer to the top surface of the enclosure when the inner cylinder is positioned close to the bottom wall. The same is true for the largest aspect ratio considered in the current study.

As the cylinder location is varied with the diagonal line for the enclosure, a noticeable distortion in the isotherms and an asymmetry in the regions above and below the inner cylinder are observed. Moreover, the results for the local Nusselt number showed that along the surface of the heated cylinder, peaks occur at the top part of the cylinder at the highest considered aspect ratios when the cylinder location is changed in the vertical direction. The same peaks are also observed when the Centre of the cylinder is changed along the diagonal line.

Only a slight difference is observed in the average Nusselt Number for different aspect ratios considered in the current study. In addition, as the aspect ratio increases, the average Nusselt Number increases.

Nomenclatures

D=R/L	Aspect ratio
h	Coefficient of heat transfer, W/m^2.°C
J	Jacobian
K	Air thermal conductivity, W/m.°C
L	Enclosure length, cm
Nu	Nusselt number
P	Pressure, N/m^2 or Function of the coordinate control
Pr	Number of Prandtl, (ν/α)
Q	Function of the coordinate control
q	Heat flux, W
Ra	Number of Rayleigh, (gβΔTD^3/να)
T	Temperature, °C
u	Velocity in x-direction, m/s
v	Velocity in y-direction, m/s
W	Enclosure width, cm
X	Dimensionless horizontal direction in physical domain
x	Horizontal direction in physical domain, m
Y	Dimensionless vertical direction in physical domain
y	Vertical direction in physical domain, m

Greek Symbols

α	Fluid thermal diffusivity, m^2/s
α, β, Γ	Parameters of transformation
β	Thermal expansion Coefficient, 1/°C
θ	Dimensionless temperature
ξ, η	Horizontal and vertical direction in computational domain
υ	Kinematic viscosity, m^2/s
φ	Dependent variable
Ψ	Stream Function, m^2/s
ω	Vorticity

Subscript

c	Cold
h	Hot
t	Time, Sec.

Superscript

-	Average
*	Dimensionless

References

1. Man, Y.H.; Kim, I.-K.; Yoon, H.S.; and Lee, S. (2002). Unsteady fluid flow and temperature fields in a horizontal enclosure with an adiabatic body. *American Institute of Physics*, 14(1), 3189-3202.

2. Man, Y.H.; Kim, I.-K.; Yoon, H.S.; and Yoon, K.S. (2002). Two-dimensional and unsteady natural convection in a horizontal enclosure with a square body. *Numerical Heat Transfer Applications*, Part A, 41(2), 183-210.
3. Jae, R.L.; and Man, Y.H. (2006). Numerical simulation of natural convection in a horizontal enclosure with a heat-generating conducting body. *International Journal Heat and Mass*, 49(1), 2684-2702.
4. Lee, J.R.; Ha, M.Y.; Balachandar, S.; and Yoon, H.S. (2004). Natural convection in a horizontal layer of fluid with a periodic array of square cylinders in the interior. *Physics of Fluids*, 16(4), 1097-1117.
5. Misra, D.; and Sarkar, A. (1997). Finite element analysis of conjugate natural convection in a square enclosure with a conducting vertical wall. *Computer Methods in Applied Mechanics and Engineering*, 141 (3-4), 205-219.
6. Wright, J.L.; Jin, H.; Hollands K.G.T.; and Naylorc, D. (2005). Flow visualization of natural convection in a tall, air-filled vertical cavity. *International Journal Heat and Mass*, 49(5-6), 889-904.
7. Pinto, R.; Paulo, M.G.; and Genésio, J.M. (2016). Numerical study of natural convection in square cavity with inner bodies using finite element method. *Journal of Fluid Dynamics*, 6(2), 75-87.
8. Vitor, J.R.; and Jian, S.U. (2015).Computational simulation of natural convection in a square cavity containing a hot cylinder. *International Nuclear Atlantic Conference.* Brazil, 4-9.
9. Abdulkadhim, A.; Al-Farhany, K.; and Abed, A.M. (2018). Effect of adiabatic circular cylinder on the natural convection heat transfer characterizes in a porous enclosure. *The Italian Association of Chemical Engineering (AIDIC)*, 71(1), 1309-1314.
10. Salam, H.H.; and Ahmed, K.H. (2010). Numerical investigation of natural convection phenomena in a uniformly heated circular cylinder immersed in square enclosure filled with air at different vertical locations. *International Communications in Heat and Mass Transfer*, 37(8), 1115-1126.
11. Cho, C.H.; Chang, K. S.; and Park, K.H. (1982). Numerical simulation of natural convection in concentric and eccentric horizontal cylindrical annuli. *Transactions of the ASME*, 104(4), 624-630.
12. Asan, H. (2000). Natural convection in an annulus between two isothermal concentric square ducts. *International Journal Heat and Mass Transfer*, 27(3),367-376.
13. Arnab, K.D.; and Amaresh, D. (2006). A numerical study of natural convection around a square, horizontal, heated cylinder placed in an enclosure. *International Journal Heat and Mass*, 49(23-24), 4608-4623.
14. Nasrine, K.; and Ghaddar, L. (1992). Natural convection heat transfer between a uniformly heated cylindrical element and its rectangular enclosure. *International Journal Heat and Mass Transfer*, 35(10), 2327-2334.
15. Moukalled, F.; and Acharya, S. (1996). Natural convection in the annulus between concentric horizontal circular and square cylinders. *Journal of Thermophysics and Heat Transfer*, 10(3), 524- 531.
16. Ding, H.; Shu, C.; Yeo, K.S.; and Lu, Z.L. (2001). Numerical study of natural convection in eccentric annuals between a square outer cylinder and circular

inner cylinder using DQ method. *International Journal Heat and Mass Transfer*, 44(4), 3321-3333.

17. Kim, B.S.; Lee, D.S.; Ha, M.Y.; and Yoon, H.S. (2008). A numerical study of natural convection in a square enclosure with a circular cylinder at different vertical locations. *International Journal Heat and Mass Transfer*, 51(1), 1888-1906.
18. Lee, J.M.; Ha, M.Y.; and Yoon, H.S. (2010). Natural convection in a square enclosure with a circular cylinder at different horizontal and diagonal locations. *International Journal of Heat and Mass Transfer*, 53(1), 5905-5919.
19. Abdulkadhim, A.; Al-Farhany, K.; and Abed, A.M.(2018). Effect of adiabatic circular cylinder on the natural convection heat transfer characterizes in a porous enclosure. *Chemical Engineering Transactions*, 71(1), 1309-1314.
20. Ali, F.H.; Hamzah, H.K.; and Abdulkadhim, A. (2018). Numerical study of mixed convection nanofluid in an annulus enclosure between outer rotating cylinder and inner corrugation cylinder. *Heat Transfer - Asian Research*, 48(1), 343-360.
21. Abdulkadhim, A.; Hamzah, H.K.; Ali, F.H.; Abed, A.M.; and Abed, M.I. (2019). Natural convection among inner corrugated cylinders inside wavy enclosure filled with nanofluid superposed in porous-nanofluid layers. *International Communications in Heat and Mass Transfer*, 109, 1-13.
22. Thompson, J.F.; Warsi, Z.U.; and Mastin, C.W. (1985). Numerical grid generation, *North-Holland*, 33(2), 188-235.
23. Van der Vorst, H.A. (1992). Bi-CGSTAB: A fast and smoothly convergence variant of BI-CG for the solution of non-symmetric linear systems. *Society for Industrial and Applied Mathematics*, 13(2), 631-644.